Parametric Analysis of the Long-Term Response of a Semi-Integral Bridge Abutment under Cyclic Thermal Movements

Pedro H. S. Silva[1]; Yuri D. J. Costa, Ph.D.[2]; Carina M. L. Costa, Ph.D.[3]; and Jorge G. Zornberg, Ph.D., P.E., F.ASCE[4]

Abstract: This paper presents the results of a parametric analysis conducted to assess relevant aspects of the long-term cyclic response of the backfill-abutment system of a semi-integral bridge located in Texas. A two-dimensional finite-element model was developed using the software Plaxis 2D version 2016 to analyze the influence of the completion season of the bridge construction, the stiffness of the bridge foundation, and the lateral displacement amplitude of the bridge abutment on the development of lateral earth pressures on the abutment and settlements on the backfill surface. The analysis was performed by considering the bridge subjected to annual temperature variations over a 50-year period. The outcome of the present investigation indicated a clear influence of the completion season of the bridge construction in the lateral earth pressures in the initial cycles, but the effect vanished in the long term. The completion season of bridge construction affected the settlements throughout the entire 50-year period. Completing the bridge construction in the summer season led to the largest settlements compared with other seasons, while winter was found to be the best period to complete the construction to prevent settlements. Increasing the bridge foundation stiffness reduced both pressures and settlements only slightly. Lower displacement amplitudes caused earth pressures to decrease with the cycles, while higher displacement amplitudes led to an increase of pressures in the initial cycles, followed by a tendency of stabilization in the long term. Conversely, all investigated amplitudes resulted in a continuous increase of settlements with the cycles. Lateral earth pressures continuously increased with increasing amplitude, while settlements escalated at a high rate under small amplitudes and tended to stabilize under large amplitudes. Soil shearing prevailed over soil densification under low amplitudes, while a balance between both shearing and densification was reached under high amplitudes. **DOI: 10.1061/JBENF2.BEENG-7064**.

Author keywords: Bridge abutment; Semi-integral bridge; Bridge construction completion season; Foundation stiffness; Lateral displacement amplitude.

Introduction

Disadvantages related to expansion joints have encouraged the use of integral abutment bridges (IABs) and semi-integral abutment bridges (SIABs) as an alternative to conventional abutment bridges. Both IABs and SIABs are structures in which the superstructure is totally integrated to the abutments. The main difference between IABs and SIABs relies on the mode of integration between the superstructure-abutment system and the bridge foundation. While IABs are constructed without expansion joints and bearing pads, resulting in a fully integrated continuous system (Husain and Bagnariol 1996; Burke 2009), SIABs are built without expansion joints, but with bearing pads, which results in a continuous system not fully connected to the foundation (Husain and Bagnariol 1999; Burke 2009). However, the lack of expansion joints can lead to lateral earth pressures on the abutment in excess of those predicted by earth pressure theories, as well as settlements on the ground surface that may compromise the safety of road users (Banks and Bloodworth 2018; Caristo et al. 2018; Abdel-Fattah and Abdel-Fattah 2019; Al-qarawi et al. 2020).

Several studies have been conducted to address the problems associated with integral bridge abutments undergoing lateral cyclic loading. Investigations have involved both field instrumentation (Breña et al. 2007; Frosch and Lovell 2011; Kim and Laman 2012; Huntley and Valsangkar 2013; Alhowaidi et al. 2023) and numerical and physical modeling (Gabrieli et al. 2015; Banks and Bloodworth 2018; Caristo et al. 2018; Abdel-Fattah and Abdel-Fattah 2019; Al-qarawi et al. 2020; Zadehmohamad et al. 2021; Liu et al. 2022; Farhangi et al. 2023). Results from these investigations have shown that the lateral earth pressures on the abutment wall and the settlements of the retained backfill surface increase with an increasing number of cycles. These observed trends have been associated with densification, rearrangement of particles, and flow of particles in the backfill soil caused by the

[1]Ph.D. Candidate, Research Institute on Mines and the Environment, Univ. of Quebec at Abitibi-Temiscamingue, 445 Blvd de l'Universite, Rouyn-Noranda, QC, Canada J9X 5E4 (corresponding author). ORCID: https://orcid.org/0000-0002-0903-1562. Email: pedrohenrique.dossantossilva@uqat.ca

[2]Professor, Dept. of Civil Engineering, Federal Univ. of Rio Grande do Norte, Av Sen Salgado Filho, 3000, Natal, RN 59072-970, Brazil. ORCID: https://orcid.org/0000-0003-2647-6931. Email: yuri.costa@ufrn.br

[3]Associate Professor, Dept. of Civil Engineering, Federal Univ. of Rio Grande do Norte, Av Sen Salgado Filho, 3000, Natal, RN 59072-970, Brazil. ORCID: https://orcid.org/0000-0002-6213-6822. Email: carina.costa@ufrn.br

[4]Professor and Joe J. King Chair in Engineering, Dept. of Civil, Architectural and Environmental Engineering, Univ. of Texas at Austin, 301E Dean Keeton St, Stop C1792, Austin, TX 78712-1174. ORCID: https://orcid.org/0000-0002-6307-1047. Email: zornberg@mail.utexas.edu

Note. This manuscript was submitted on May 20, 2024; approved on December 19, 2024; published online on February 27, 2025. Discussion period open until July 27, 2025; separate discussions must be submitted for individual papers. This paper is part of the ***Journal of Bridge Engineering***, © ASCE, ISSN 1084-0702.

cyclic movements of the abutment. Findings from these studies provide the baseline data to conduct further investigations on the behavior of semi-integral bridge abutments in need of elucidation.

While progress has been made in understanding the cyclic response of backfill-abutment systems of integral bridges, limited attention has been paid to semi-integral systems. Semi-integral bridge abutments have been reported to present some advantages over integral abutments. For example, semi-integral connections give the superstructure some freedom of movement in the longitudinal direction, which reduces stresses and moments transferred to supporting piles and prevents damage upon cycling during the bridge lifespan (Arsoy et al. 2002, 2004). Additionally, semi-integral connections minimize the effects of differential longitudinal forces on the abutment, which allows higher skew angles and requires less restrictive subsurface conditions (Husain and Bagnariol 1999; Burke 2009).

Despite these advantages, the use of semi-integral bridges is still small compared with integral bridges. In the academic field, there is a reduced number of publications on semi-integral bridges, the majority of which concentrate on the structural features of the bridge (Shid Moosavi and Rahai 2018; Hussein et al. 2022; Ahmed et al. 2023), while important geotechnical aspects are set aside. Among the geotechnical investigations, the greatest interest has been in the lateral earth pressure behavior upon cyclic movements, and other important aspects, such as backfill settlements and deformations, failure mechanisms developments, displacement amplitude effects, bridge foundation stiffness effects, and bridge construction completion (the moment in which the bridge project is considered completed and ready for use) season effects, have been overlooked.

Steinberg et al. (2004) monitored the wing walls of two skewed semi-integral bridges for approximately 1 year and noted a nonlinear increase in the horizontal forces on the wing walls due to longitudinal movements of the bridge. Hoppe and Bagnall (2008) monitored a highly skewed semi-integral bridge for a 17-month period and recorded significant variations in the lateral earth pressures at the back wall and wing walls in the lateral direction. The authors related these significant variations to the predominant movement direction, which is along the long diagonal, of thermally induced expansion and contraction at the skewed superstructure. Also, cracks were observed at the wing wall as a consequence of an unbalanced passive earth pressure. Kim et al. (2014) monitored a semi-integral bridge for about 3 years and observed a slight increase in the lateral earth pressures on the abutment with temperature fluctuation cycles. The authors attributed this change to the poor backfill compaction and the low height of the abutment. Huang et al. (2022) conducted small-scale physical model tests on a semi-integral bridge abutment subjected to cyclic lateral loading and noted an increase in the lateral earth pressures behind the abutment with the cycles. The increase rate gradually slows down cycle by cycle, and this behavior was associated with the gradual compaction experienced by the soil mass with an increasing number of cycles.

Accordingly, this paper presents a parametric analysis to investigate relevant aspects of the long-term cyclic behavior of the backfill-abutment system of a semi-integral bridge subjected to temperature fluctuations. A two-dimensional finite-element (FE) model was developed to analyze the influence of the completion season of the bridge construction, the stiffness of the bridge foundation, and the lateral displacement amplitude of the bridge abutment on the development of lateral earth pressures on the abutment and settlements of the backfill surface upon cycling. The study represents a 50-year period of annual cycles of expansion–contraction of the bridge superstructure.

Methodology

The bridge evaluated in this study is a semi-integral, stub-type concrete bridge, with a length of 20.53 m and a width of 7.85 m, located at Anderson County, in Texas where Road 2133 crosses the Mack Creek (Fig. 1). The bridge superstructure, which is integrally connected to 1.05-m high and 0.3-m-thick-reinforced concrete abutments, is composed of a 0.15-m-thick-reinforced concrete deck supported on 0.5-m-high prestressed concrete box beams. The superstructure-abutment system is supported by 6.6-m-long-driven PZC-18 steel sheet piles, connected to 0.83-m-wide and 0.75-m-high reinforced concrete pile caps. The space between the abutments and the pile caps was filled out with a 40-mm-thick preformed bituminous fiber material (PBFM), while a 70-mm-thick laminated elastomeric bearing pad (LEBP) was placed between the pile caps and the bridge superstructure. Wing walls composed of 2.1-m-long-driven PZC-18 steel sheet piles were built normal to the abutments to retain the backfill material. The backfill material in contact with the bridge

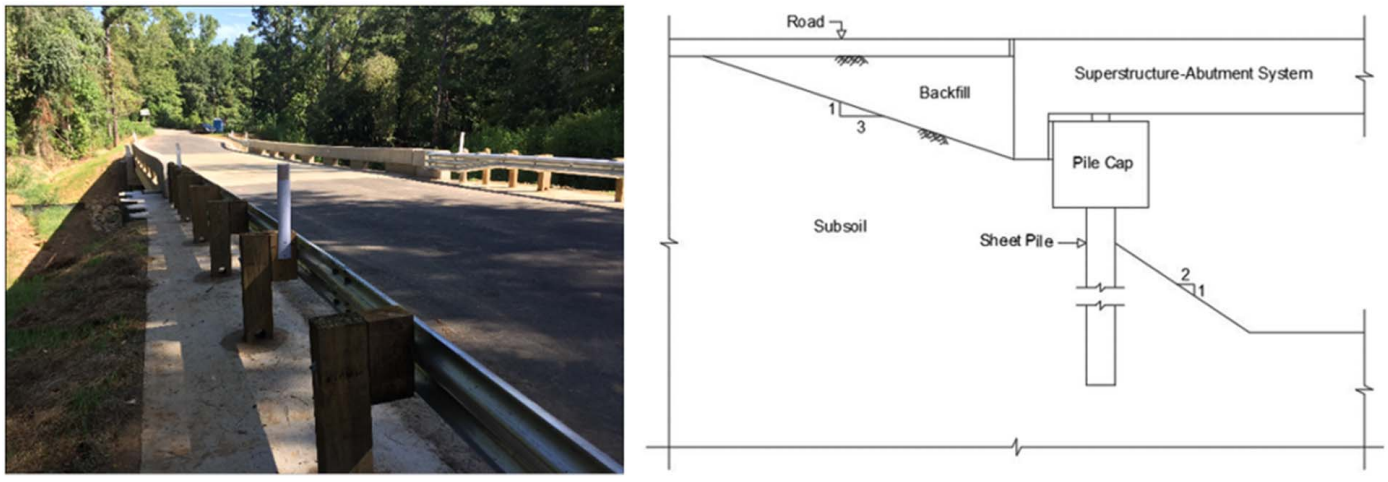

Fig. 1. (a) Photograph of the semi-integral bridge after completion of construction (image by Jorge G. Zornberg); and (b) schematic elevation view of the bridge in the region of the abutment.

J. Bridge Eng., 2025, 30(5): 04025021

abutment consists of a clean, poorly graded gravel (GP), and the natural ground is composed of a sandy soil layer overlying a clayey soil layer. Further details about the bridge properties and subsoil conditions can be found in Silva et al. (2023).

The proposed numerical study was carried out with a plain-strain FE model of the north abutment, developed with the software Plaxis 2D version 2016 (Brinkgreve et al. 2016). Fig. 2 shows the geometry of the proposed numerical model. The mesh size extended to a length of 40 m in the horizontal direction and 20 m in the vertical direction. The model is composed of a 6.35-m-thick silty sand layer over a 13.5-m-thick sandy clay layer, with a triangular-shaped gravel backfill in contact with the abutment wall. The soil and concrete materials were modeled by using a mesh containing 4,410 15-node triangular solid elements, while the foundation sheet piling was modeled by using plate elements. Because approach slabs were not used in the bridge built in Texas, the modeling of approach slabs above the backfill was not considered in the present investigation. The lateral boundaries of the mesh are free to move in the vertical direction and fixed in the horizontal direction, while the base of the mesh is constrained from moving in both vertical and horizontal directions. Further details about the FE model can be found in Silva et al. (2023).

The stress–strain behavior of the soil and the structural materials was modeled, respectively, by using the hardening soil (HS) constitutive model (Schanz et al. 1999) and by an isotropic linear–elastic relationship. A power coefficient for the stress-level dependency of stiffness (m) of 0.5 was adopted for the soil materials. The soil–structure interface properties were taken into account by using strength reduction factors (R_{inter}) of 0.5 for the soil–steel interface and 0.7 for the soil–concrete interface (Silva et al. 2023).

The soil properties were defined based on the results of laboratory and Texas Cone Penetrometer (TCP) tests, as well as on relevant correlations, as discussed by Silva et al. (2023). Parameters assigned for the backfill gravel were adopted using the results from a series of conventional consolidated isotropically drained (CID) triaxial tests, while parameters attributed for the silty sand and the sandy clay layers were defined from the results of TCP tests. Specifically, the undrained shear strength for the sandy clay layer was estimated as $2.15N_{\text{TCP}}$ (kPa), where N_{TCP} is TCP blow-count resistance, as suggested by Vipulanandan et al. (2008), and the effective friction angle for the silty sand layer was estimated from recommendations reported in TxDOT (2020).

In summary, unit weight (γ) values of 19, 17, and 20 kN/m^3 were adopted for the sandy clay, the silty sand, and the gravel, respectively. Reference drained Young's modulus at 50% of maximum strength (E_{50}^{ref}) of 60, 40, and 30 MPa were assigned to the sandy clay, the silty sand, and the gravel, respectively. An undrained shear strength (S_u) of 210 kPa was assumed for the sandy clay, and peak effective friction angles (ϕ'_p) of 31.5° and 43° were assumed for the silty sand and the gravel, respectively. Additionally, a dilatancy angle (ψ) of 10° was considered for the gravel, and an effective cohesion (c') of 15 kPa was assumed for the silty sand. The following properties were adopted for the reinforced concrete: unit weight (γ) of 25 kN/m^3, Young's modulus (E) of 30 GPa, and Poisson's ratio (ν) of 0.2. The following parameters were set to the sheet pile: weight per unit length (w) = 1.16 kN/m/m, axial stiffness (EA) = 3.16×10^6 kN/m, flexural stiffness (EI) = 7.33×10^4 kNm^2/m, and Poisson's ratio (ν) = 0.3. Further details about the soil properties can be found in Silva et al. (2023).

Temperature-induced cyclic loads were incorporated in the numerical model by imposing prescribed horizontal displacements at the top of the abutment to simulate the effects of expansion and contraction of the superstructure due to temperature fluctuations. Bridge length changes (ΔL) due to temperature variation were predicted as follows (AASHTO 2017):

$$\Delta L = \alpha \cdot L \cdot \Delta T \tag{1}$$

where α = thermal expansion coefficient of the bridge material, assumed equal to 10.8×10^{-6} °C^{-1} (AASHTO 2017); L = bridge length; and ΔT = bridge temperature variation. The prescribed horizontal displacements were calculated by dividing the predicted ΔL value by 2 (this assumption is believed to be in accordance with field conditions since both backfills were built with the same material). Further details about the implementation of temperature-induced cyclic loads in the numerical model can be found in Silva et al. (2023).

A total of 50 cycles of lateral displacements of the abutment were assigned to simulate the bridge behavior over a 50-year period. Daily cycles were ignored in the numerical simulations, since daily temperature changes are expected to be much smaller than seasonal temperature changes (Liu et al. 2022). Eliminating daily cycles is assumed to have negligible impact on long-term analyses and has been widely adopted by similar studies on integral and semi-integral bridge abutments to reduce computational time (Caristo et al. 2018; Abdel-Fattah and Abdel-Fattah 2019; Zadehmohamad et al. 2021; Liu et al. 2022; Ahmed et al. 2023; Farhangi et al. 2023). Springman et al. (1996) concluded that daily temperature cycles were not more critical to design than annual temperature cycles. England et al. (2000) noted that the overall effect of daily and seasonal temperature variations was comparable to that of seasonal temperature variations alone. Banks and Bloodworth (2018) observed an increase of only 10% in the soil stresses between a long-term analysis with daily cycles within the annual behavior and an analysis with the same time span but with annual cycles only. However, the more conservative result with the daily cycles was attributed to the intrinsic features of the soil model used.

The variables selected for investigation were the season of the year when bridge construction is completed, the stiffness of the bridge foundation, and the amplitude of the lateral displacement. The completion season of the bridge construction was studied for an imposed lateral displacement (d) of ± 5 mm, which corresponds to a normalized lateral displacement (d/h) of ± 0.5% (where h is the abutment height in contact with the backfill). The magnitude of the imposed lateral displacement (d) was obtained by assuming a temperature amplitude equal to 45°C, according to AASHTO's (2017) recommendations for the location of the bridge.

The sequence of lateral displacements in an annual cycle for the four seasons of the year is depicted in Fig. 3. The bridge abutment completed in the spring season displaces $d/2$ toward the backfill from spring to summer, d away from the backfill from summer to winter, and $d/2$ toward the backfill from winter to spring [Fig. 3(a)]. The bridge abutment completed in summer displaces d away from the backfill from summer to winter and d toward the backfill from winter to summer [Fig. 3(b)]. Accordingly, the bridge abutments completed in autumn and in winter displace in the opposite way to those completed in spring and in summer, respectively [Figs. 3(c and d)].

The effect of the bridge foundation stiffness was evaluated for three different sheet pile profiles manufactured by Gerdau, which are PZC-12, PZC-18, and PZC-28. Table 1 presents the structural parameters of the selected sheet pile profiles, according to Gerdau (2019). The same lateral displacement amplitude assumed for the completion season of the bridge construction was applied to this analysis (i.e., d/h equal to ± 0.5%). The displacement sequence followed that of the bridge completed in summer, since the construction of the Mack Creek bridge was concluded in July (Zornberg et al. 2019).

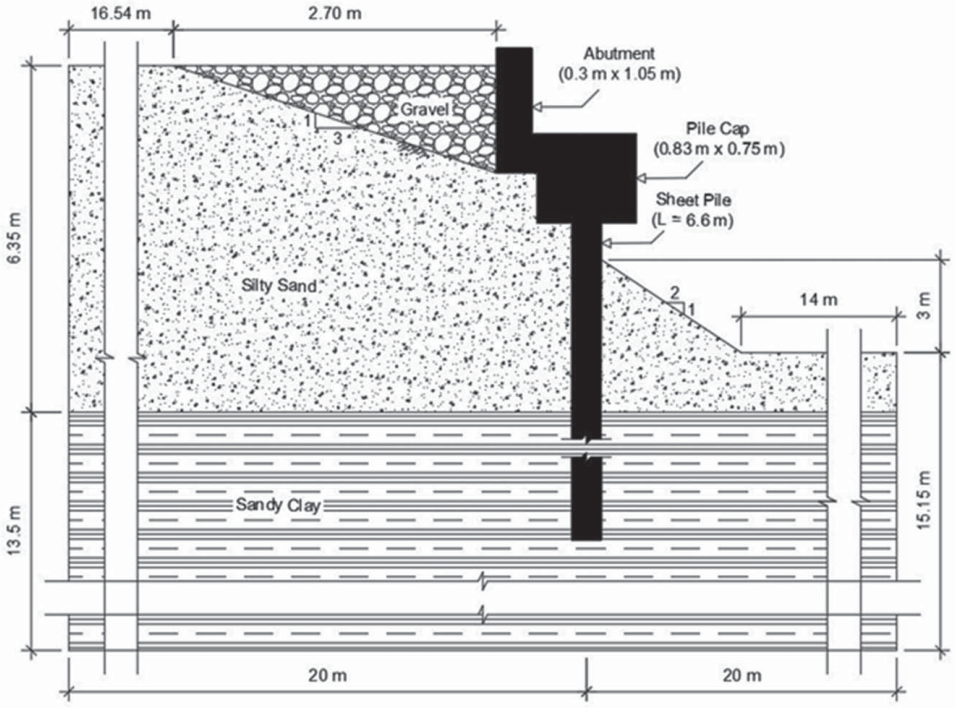

Fig. 2. Numerical model geometry.

The impact of the lateral displacement amplitudes of the bridge abutment was assessed for d/h equal to ±0.1%, ±0.2%, ±0.3%, ±0.4%, and ± 0.5%. These values were chosen based on previous numerical and experimental investigations (Ng et al. 1998; Bloodworth et al. 2012; Civjan et al. 2013; Huntley and Valsangkar 2013; Mitoulis et al. 2016; Caristo et al. 2018). The summer displacement sequence was assumed to this analysis as well.

The phases considered in the numerical simulations included: (1) calculation of the initial geostatic stresses in the subsoil; (2) installation of the structural elements, placement of the granular

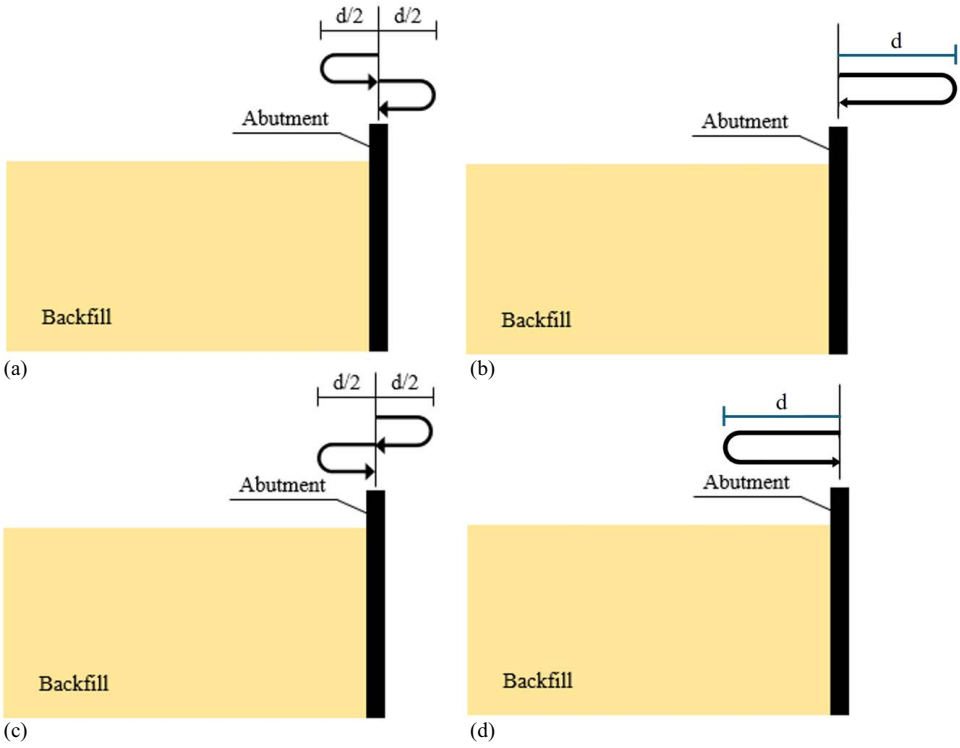

Fig. 3. Lateral displacements of a bridge abutment for the four different completion seasons of construction along the year: (a) spring; (b) summer; (c) autumn; and (d) winter.

Table 1. Structural parameters of sheet pile profiles

Parameter	Profile		
	PZC-12	PZC-18	PZC-28
Poisson's ratio, ν	0.3	0.3	0.3
Axial stiffness, EA (kN/m)	2.61×10^6	3.16×10^6	4.44×10^6
Flexural stiffness, EI (kN · m^2/m)	4.01×10^4	7.33×10^4	1.30×10^5
Weight per unit length, w (kN/m/m)	0.98	1.16	1.66

Note: A = cross-sectional area of a sheet pile; and I = moment of inertia of a sheet pile.

backfill and application of the loads on the abutment, pile cap and backfill; and (3) application of the sequential lateral displacements on the abutment.

Model Validation

The numerical model was validated against data collected in the field. Prescribed horizontal displacements were applied to the abutment to simulate the temperature-induced cyclic lateral movements induced by daily maximum expansions and contractions of the bridge superstructure. The corresponding lateral earth pressures were then compared with readings recorded from earth pressure cells installed on the bridge abutment wall. Fig. 4 compares predicted and measured lateral earth pressure values for 100 daily cycles. The maximum and minimum values of lateral earth pressures presented in Fig. 4 correspond to those obtained for the daily maximum expansions and contractions of the bridge superstructure, respectively. It is observed that field and numerical data showed a close relationship, with very small discrepancies. The corresponding Pearson's product-moment correlation coefficient (r) was equal to 0.905, indicating a very strong correlation between both variables (Salkind 2017). Additional information on the model validation can be found in Silva et al. (2023).

Results and Discussion

Influence of the Completion Season of Bridge Construction

Fig. 5 shows the peak wall reaction ratio (K_{wp}) for selected annual cycles, considering the four completion seasons of the bridge construction. The values of K_{wp} were defined according to the following equation (England et al. 2000):

$$K_{wp} = \frac{P_{\max}}{0.5\gamma h^2} \tag{2}$$

where $P_{\max}$ = maximum total soil lateral force acting on the abutment wall per unit length; γ = unit weight of the backfill material; and h = abutment height in contact with the backfill (0.9 m). It is noted that, for all four scenarios, K_{wp} presented a significant increase in the first cycles, followed by stabilization. A clear effect of the completion season of the bridge construction is noted in the initial cycles only. The effect vanished from the fifth cycle onward, and K_{wp} remained virtually uninfluenced by the completion season. Similar results were reported by England et al. (2000) and Caristo et al. (2018).

Fig. 6 shows the normalized maximum backfill settlement ($\rho_{\max}/h$) for different completion seasons of the bridge construction. The maximum settlement ($\rho_{\max}$) was obtained where the backfill surface meets the abutment wall face. It is noted that $\rho_{\max}/h$ presented a significant increase with the cycles, with no tendency for stabilization. Differently from the lateral earth pressures, the settlements were found to be highly affected by the construction completion season. The largest settlements took place for the bridge

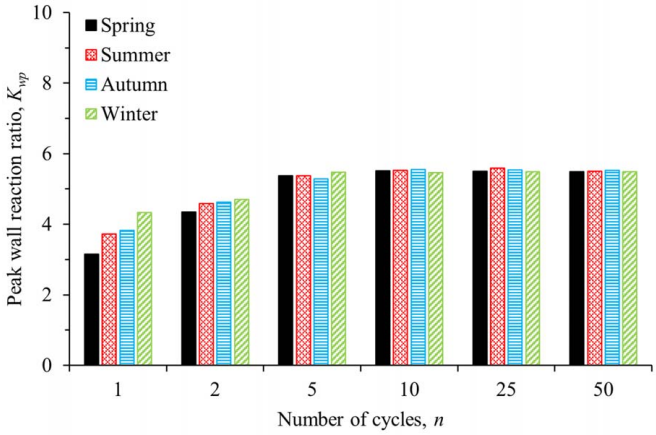

Fig. 5. Peak wall reaction ratios for selected annual cycles, considering different completion seasons of bridge construction.

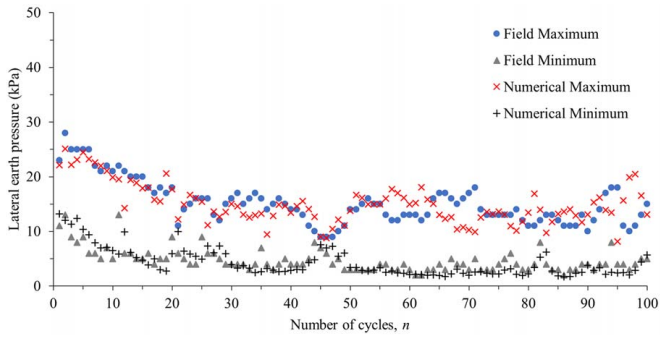

Fig. 4. Comparison between predicted and measured lateral earth pressures.

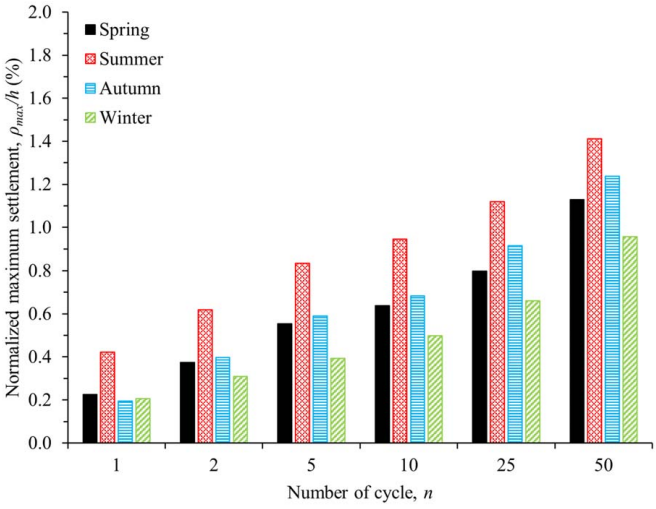

Fig. 6. Normalized maximum settlements for selected annual cycles, considering different completion seasons of bridge construction.

completed in summer, while the smallest settlements occurred in winter. Accordingly, intermediate settlements were found for spring and autumn. At Cycle no. 50, settlements for the bridge completed in winter were about 47% smaller than settlements for the bridge completed in summer.

When the abutment initially displaces away from the backfill (active mode) (i.e., bridge construction completed in summer or in autumn), the soil near the structure first undergoes a decompression when it slips downward to fill the gap that formed between the abutment and the backfill. In this case, the reduction in stiffness experienced by the soil mass tends to magnify settlements on the backfill surface at the end of the cycle. On the other hand, when the abutment initially displaces against the backfill (passive mode) (i.e., bridge construction completed in winter or in spring), the soil mass near the abutment wall is first pushed against the undisturbed soil far from the structure, which makes it denser. In this situation, the increase in stiffness experienced by the soil mass tends to diminish surficial settlements at the end of the cycle.

The findings from the present study contrast with results from other studies. Numerical simulations carried out by England et al. (2000) showed that the largest settlements occurred with the bridge construction completed in winter. On the other hand, Caristo et al. (2018) demonstrated, also with numerical simulations, that settlements were not influenced by the completion season of bridge construction. The discrepancy between the results of these two studies and the results of the present work can be explained by the different characteristics of the numerical models used in each case. England et al. (2000) modeled a part of an integral abutment subjected to rotation movements only, while Caristo et al. (2018) modeled a complete integral abutment undergoing combined movements of rotation and translation. On the other hand, in the present investigation, a semi-integral abutment experiencing both rotation and translation movements was modeled. Furthermore, in contrast to the present investigation, the effects of the superstructure and the approach road were ignored in the studies of both England et al. (2000) and Caristo et al. (2018).

The results obtained in the present study encourage the assessment of the influence of the completion season of the bridge construction in the design phase of semi-integral abutment bridges, since it may affect the safety of road users and the road riding quality. For the specific case under evaluation, the conclusion of the bridge in summer would be the most unfavorable scenario for the development of settlements on the backfill surface, which would require earlier and more frequent maintenance programs in comparison with the other seasons. As a matter of fact, field inspections carried out during the first 3 years after the opening of the Mack Creek bridge to traffic visually confirmed, in both abutments, the formation of a noticeable depression between the approach road and the bridge deck, as well as a gap between the wing wall and the abutment (Mofarraj and Zornberg 2022).

Influence of the Stiffness of the Bridge Foundation

The behavior of K_{wp} and ρ_{max}/h with the cycles for different sheet pile profiles is shown in Figs. 7 and 8, respectively. It is noted that K_{wp} significantly increased within the first cycles, and then, it tended to stabilize (Fig. 7), while ρ_{max}/h increased continuously with the cycles and showed no tendency for stabilization (Fig. 8). It can be also noted that an increase in the sheet piling stiffness caused a very discrete impact on the reduction of stresses and settlements on the backfill-abutment system. While replacing Profile PZC-12 with Profile PZC-28 results in an increase of 224% in the flexural stiffness (EI), it represents a reduction of only 8% in K_{wp} and 5% in ρ_{max}/h at Cycle no. 50.

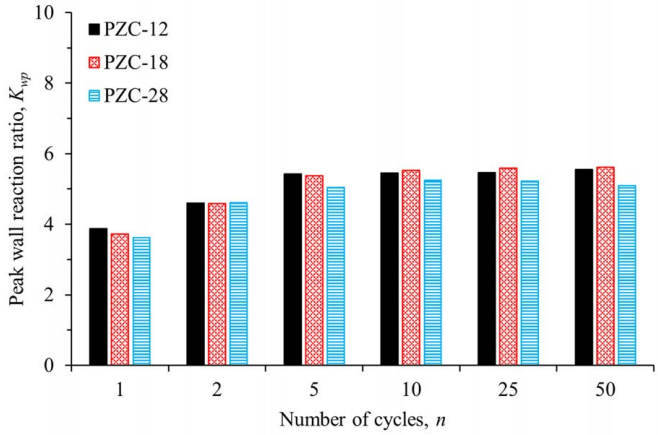

Fig. 7. Peak wall reaction ratios for selected annual cycles and different sheet pile profiles.

The small influence of the sheet piling stiffness on the cyclic response of the backfill-abutment system is due to the semi-integral connections between the abutment-superstructure system and the foundation system of the bridge, which contributes to alleviate the forces caused by the cyclic extension-contraction movements of the bridge's superstructure. The Mack Creek Bridge has a 70-mm-thick LEBP between the pile cap and the superstructure, and a 40-mm-thick PBFM between the pile cap and the bridge abutment, which were taken into consideration in the proposed numerical model, as discussed by Silva et al. (2023). Therefore, an increase in pile stiffness is expected to play a small impact on the backfill-abutment cyclic response, as shown in Figs. 7 and 8. These findings corroborate the results of the numerical study performed by Arsoy et al. (2002), which showed that, for a constant temperature variation, the lateral displacements of piles supporting semi-integral abutments were less than those of piles supporting integral abutments.

From a design standpoint, the comparatively small influence of the pile foundation stiffness of semi-integral bridges is beneficial, since the required bridge performance could be achieved with slender pile elements. However, the choice of piling stiffness must be carefully evaluated in design to ensure a balanced approach

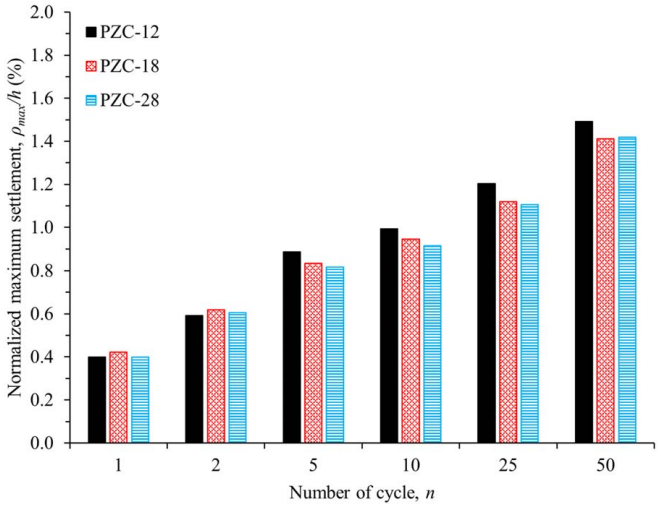

Fig. 8. Normalized maximum settlements for selected annual cycles and different sheet pile profiles.

between engineering performance and economic feasibility in the semi-integral bridge design and construction.

Influence of the Lateral Displacement Amplitude

Fig. 9 shows the variation of K_{wp} with selected annual cycles, for different lateral displacement amplitudes imposed on the bridge abutment. It is noted that K_{wp} increased with increasing imposed lateral displacement amplitude. However, K_{wp} reduced slightly with the annual cycles for the lower values of d/h of 0.1% and 0.2%, while the higher values of d/h of 0.3%, 0.4%, and 0.5% led to an increase of K_{wp} in the initial cycles, followed by a tendency to stabilize. The larger d/h, the more significant was the increase in K_{wp}. The results of Fig. 9 also suggest that there is a normalized lateral displacement, between 0.2% and 0.3%, for which K_{wp} would not be affected by the cyclic lateral displacements of the abutment.

The response of ρ_{max}/h with the annual cycles is depicted in Fig. 10 for different lateral displacement amplitudes. It is observed that ρ_{max}/h increased significantly with increasing lateral displacement amplitude, and no stabilization of ρ_{max}/h was observed for any displacement amplitude. The shape of the curves reveals a nearly linear growth of ρ_{max}/h with the cycles for lower amplitudes (i.e., $d/h = 0.1\%$ and 0.2%), while higher amplitudes (i.e., $d/h =$ 0.3%, 0.4%, and 0.5%) caused a nonlinear increase of ρ_{max}/h in the first five cycles, followed by a linear increase. The growth rate of ρ_{max}/h in the initial cycles increases with increasing displacement amplitude. The results depicted in Figs. 9 and 10 are in accordance with those reported by England et al. (2000), from small-scale physical model tests and numerical simulations.

The long-term cyclic response of the backfill-abutment system is investigated subsequently. Figs. 11 and 12 show K_{wp} and ρ_{max}/h as a function of the relative displacement amplitude (d/h) after Cycle no. 50, respectively. Cycle no. 50 was chosen because it represents the longest period in the present analysis. For reference, earth pressure coefficients calculated according to Rankine's (1857) theory for a passive earth pressure condition ($K_{p,\text{Rankine}}$) and design methods for integral bridge abutment specified in Document PD6694-1 (BSI 2011) and in Massachusetts Department of Transportation's Bridge Design Guidelines (MassDOT 2020) are also plotted in Fig. 11.

The method described in PD6694-1 (BSI 2011) assumes an earth pressure coefficient, K^*, calculated from the following

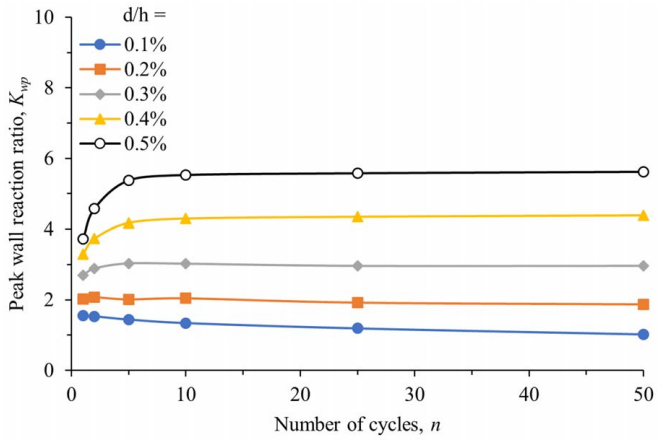

Fig. 9. Peak wall reaction ratios for selected annual cycles and lateral displacement amplitudes imposed on the bridge abutment.

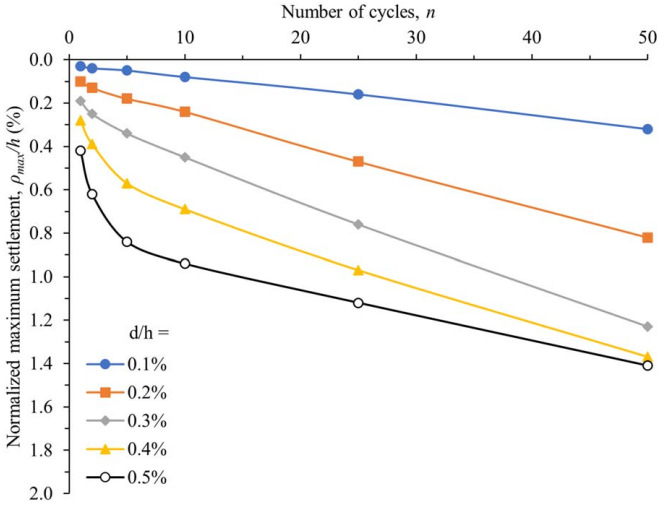

Fig. 10. Normalized maximum settlements for selected annual cycles and lateral displacement amplitudes imposed on the bridge abutment.

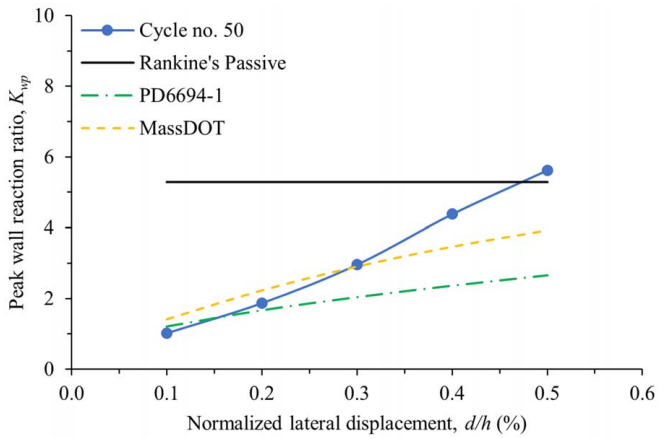

Fig. 11. Peak wall reaction ratios versus normalized lateral displacements after Cycle no. 50 and comparison with earth pressure coefficients from design guidelines.

equation:

$$K^* = K_o + \left[\left(C \times \frac{d'}{h}\right)^{0.6}\right] K_p \tag{3}$$

where K_o = at-rest earth pressure coefficient, calculated as $1 - \sin \varnothing$ (Jaky 1944); h = abutment wall height in contact with the backfill; d' = wall movement range $h/2$ below ground level, taken as 0.5 times the displacement range at the top of the abutment according to PD6694-1 (BSI 2011); K_p = passive earth pressure coefficient obtained from Eurocode 7 (BSI 2014), assuming an interface friction angle equal to $\varnothing/2$; and C = coefficient calculated from the following equation:

$$C = 0.51E_s + 14.9 \quad (20 \le C \le 66) \tag{4}$$

where E_s = backfill Young's modulus (MPa), set as 30 MPa (Silva et al. 2023). MassDOT's (2020) solution requires that an earth pressure coefficient, K_m^*, be calculated from the following empirical

relationship:

$$K_m^* = 0.43 + 5.7[1 - e^{-190(d/h)}] \quad (5)$$

where d = total displacement at the top of the abutment; and h = abutment wall height in contact with the backfill. The values of d/h were assumed equal to 0.1%, 0.2%, 0.3%, 0.4%, and 0.5% for both design guidelines.

As depicted in Fig. 11, K_{wp} exhibited a nearly linear growth with d/h. Rankine's theory for the passive condition gave good predictions of K_{wp} for the range of large amplitudes around $d/h = 0.5\%$. On the other hand, the methods by PD6694-1 (BSI 2011) and MassDOT (2020) resulted in suitable predictions of K_{wp} for the range of low amplitudes (i.e., d/h between 0.1% and 0.3%). When $d/h > 0.3\%$, results from both methods gradually moved away from the numerical results as d/h grew. The backfill response to displacement amplitude variations, in terms of long-term settlements, was meaningful, as shown in Fig. 12. Under lower amplitudes, ρ_{max}/h presented a rapid increase with d/h. After d/h around 0.3%, the growth rate of ρ_{max}/h decreased dramatically and tended to stabilize with increasing d/h.

Despite its complexity, the overall behavior of a granular backfill upon cyclic lateral displacements of the abutment can be understood in terms of volume changes (densification and/or dilatation), rearrangement of particles (fabric changes), and flow of particles (shearing) (England et al. 2000; Cosgrove and Lehane 2003; Clayton et al. 2006). Densification leads to greater homogeneity, strength, and stability of the backfill, while fabric changes and shearing inhibit volume changes, thus reducing the backfill stability (England et al. 2000). Consequently, soil densification leads to an elevation of the lateral earth pressures due to the increase in soil stiffness, while soil shearing induces a reduction in the lateral earth pressures, with both effects increasing settlements of the backfill surface (Silva et al. 2023). Experimental evidence showing soil densification and particle flow in a backfill-abutment system undergoing cyclic lateral movements can be found from the results of small-scale physical model tests with granular soils reported by several researchers (Tatsuoka et al. 2009; Gabrieli et al. 2015; Al-qarawi et al. 2020).

In the present investigation, volume changes and shearing in the backfill soil are inspected from information depicted in Figs. 13 and 14, respectively. Volume changes in the soil were evaluated from volumetric strain (ε_v) values calculated according to Eq. (6),

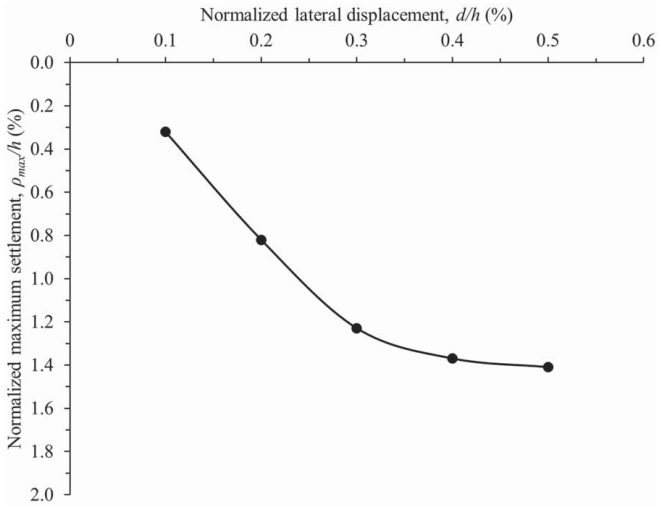

Fig. 12. Normalized maximum settlements versus normalized lateral displacements after Cycle no. 50.

while soil shearing was evaluated from deviatoric strain (γ_d) values defined according to Eq. (7) (Brinkgreve et al. 2016):

$$\varepsilon_v = \varepsilon_x + \varepsilon_y + \varepsilon_z \quad (6)$$

$$\gamma_d = \sqrt{\frac{2}{3}\left[\left(\varepsilon_x - \frac{\varepsilon_v}{3}\right)^2 + \left(\varepsilon_y - \frac{\varepsilon_v}{3}\right)^2 + \left(\varepsilon_z - \frac{\varepsilon_v}{3}\right)^2 + \frac{1}{2}(\gamma_{xy}^2 + \gamma_{yz}^2 + \gamma_{zx}^2)\right]} \quad (7)$$

where ε_x = axial strain in the x-direction; ε_y = axial strain in the y-direction ($\varepsilon_y = 0$ in plane-strain conditions); ε_z = axial strain in the z-direction; γ_{xy} = shear strain in the xy-plane; γ_{yz} = shear strain in the yz-plane ($\gamma_{yz} = 0$ in plane-strain conditions); and γ_{zx} = shear strain in the zx-plane. Fig. 13 presents shadings of cumulative volumetric strains after completion of Cycle no. 50, for the target displacement amplitudes of 0.1%–0.5%. Shadings of cumulative deviatoric strains after completion of Cycle no. 50 are shown in Fig. 14 for the same displacement amplitudes. In both figures, distances x and z are normalized by the abutment height (h) in contact with the backfill, and the origin of both x- and z-axes is placed at the abutment toe.

According to Fig. 13, the magnitude of the volumetric strains increased with increasing lateral displacement amplitudes. As the displacement amplitude increased, a zone of soil dilatation (negative volumetric strains) developed in a small region near the backfill surface, close to the abutment wall, while a comparatively large zone of soil densification (positive volumetric strains) spread below the dilatant area and concentrated at the middle third of the backfill. The densification of the soil with increasing displacement amplitude led the backfill to a gradually stiffer state, which explains the growth of K_{wp} shown in Fig. 11. Densification and dilatation of the soil were significantly less prominent with lower amplitudes of $d/h =$ 0.1% and 0.2% than with the higher amplitudes of $d/h =$ 0.3%, 0.4%, and 0.5%.

As shown in Fig. 14, the magnitude of the displacement amplitude was found to define how shearing propagates in the backfill soil. The lower amplitudes of $d/h =$ 0.1% and 0.2% led to the development of shear bands in the soil mass, propagating from specific depths along the abutment wall face and reaching the backfill surface. The shear zone was larger with $d/h = 0.2\%$ than with $d/h = 0.1\%$. Conversely, the higher amplitudes of $d/h =$ 0.3%, 0.4%, and 0.5% led to a different shearing mechanism, in which a single shear band propagated from the abutment toe and reached the backfill surface at a distance x/h equal to approximately 0.7. This mechanism also included a region of intense diffused shearing that spreads from the upper corner of the backfill and encompasses the whole sliding mass. Shearing in the soil mass was clearly more intense with lower displacement amplitudes.

The predominance of soil shearing over soil densification under the low displacement amplitudes of $d/h =$ 0.1% and 0.2% explains the reduction in the lateral earth pressures and the increase in the settlements with the cycles, as shown in Figs. 9 and 10, respectively. Both amplitudes are deemed too small to cause any significant densification of the retained soil mass. On the other hand, a more balanced effect between shearing and densification was reached with the higher amplitudes of $d/h =$ 0.3%, 0.4%, and 0.5%, which were sufficiently large to densify the soil. Stabilization of lateral earth pressures and an increase of settlements with the cycles are a consequence of this equilibrium, as can be seen in Figs. 9 and 10.

The combination of high shearing and low densification that occurred with low amplitudes (below $d/h = 0.3\%$) resulted in more instability of the backfill soil and led to a rapid increase in the long-term settlements with increasing displacement amplitude, as shown

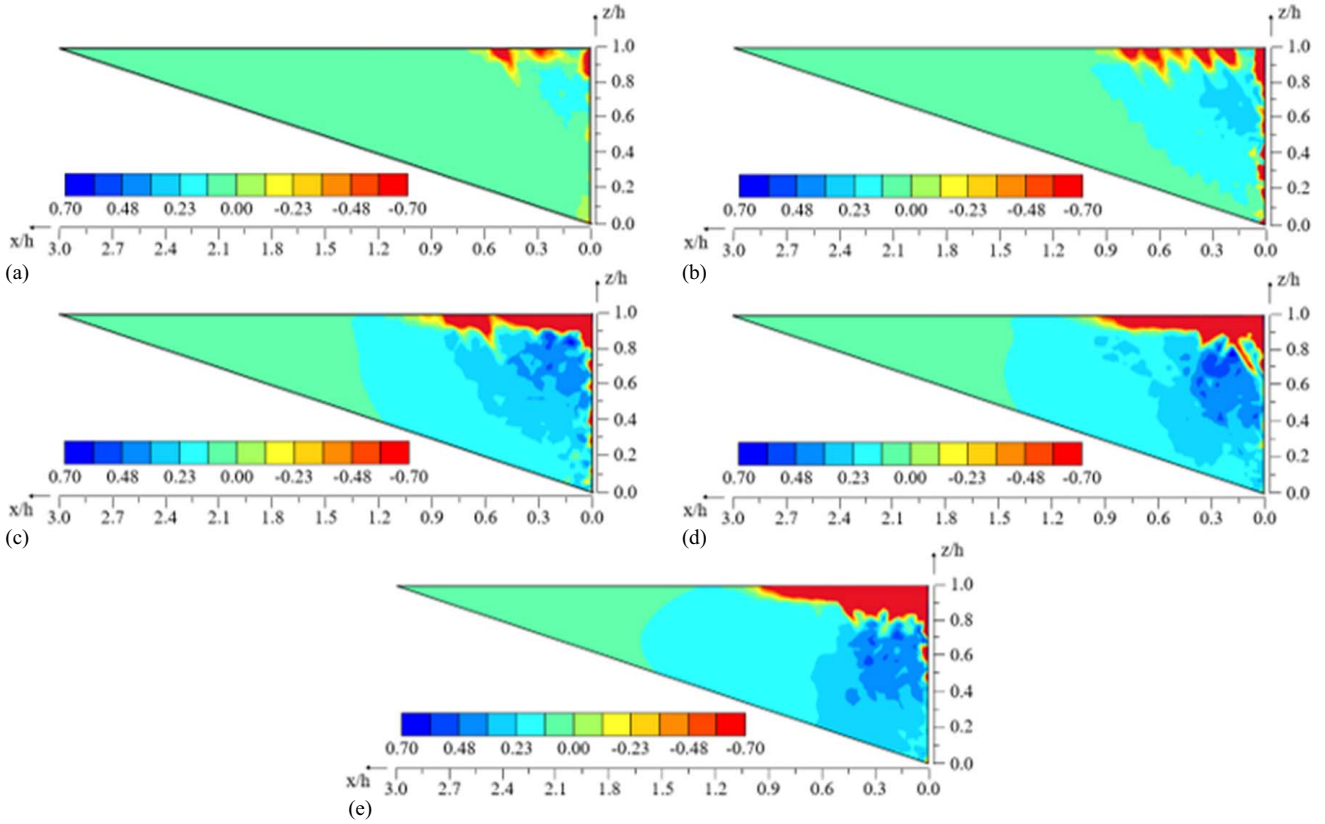

Fig. 13. Contours of cumulative volumetric strains (%) in the backfill at the end of Cycle no. 50 for *d*/*h* equal to (a) 0.1%; (b) 0.2%; (c) 0.3%; (d) 0.4%; and (e) 0.5%.

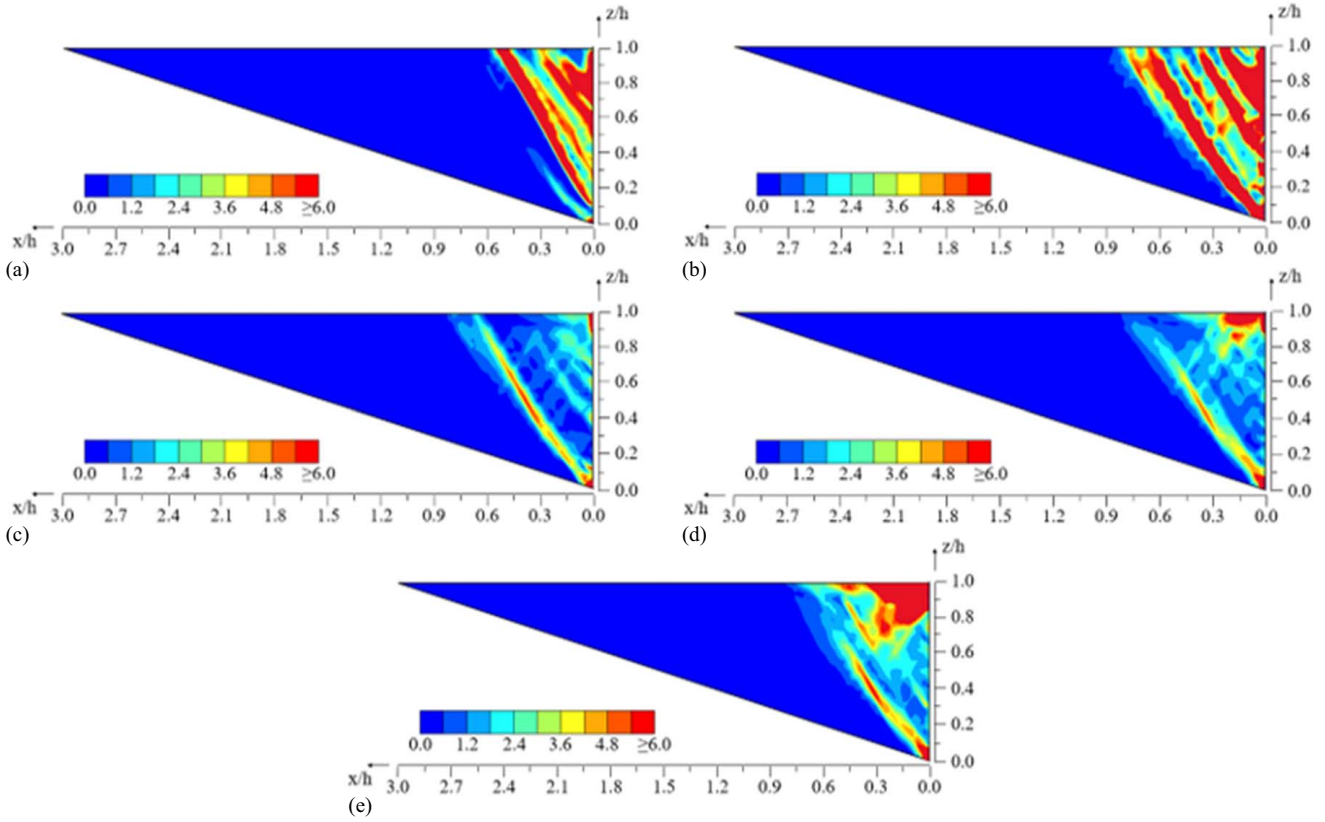

Fig. 14. Contours of cumulative deviatoric strains (%) in the backfill at the end of Cycle no. 50 for *d*/*h* equal to (a) 0.1%; (b) 0.2%; (c) 0.3%; (d) 0.4%; and (e) 0.5%.

in Fig. 12. On the other hand, the association of low shearing and high densification that took place with high amplitudes ($d/h \geq 0.3\%$) led the backfill soil to a more stable condition, which includes the stabilization of the long-term settlements with increasing amplitude. The change in the long-term settlement behavior was found to occur for an amplitude d/h of around 0.3%.

An additional analysis can be carried out to understand the effect of the bridge length on the long-term settlements of the backfill, based on the result presented in Fig. 12. Because of thermal properties, the lateral displacements generated on the abutments will be directly proportional to the length of the bridge. That is, the longer the bridge, the greater the expected lateral displacements. However, the data shown in Fig. 12 suggest that abutment backfills of shorter bridges would be more prone to settlement variations caused by changes in the lateral displacement magnitude. This would not be the case for longer bridges, for which backfill settlements would be much less dependent on lateral displacement magnitude variations. By recognizing the impact of the lateral displacement amplitude on the long-term response of the backfill-abutment system, potential damaging effects on the bridge that may arise from lateral displacement variations could be anticipated with the design of systems that could better withstand changes in loading conditions over time.

Conclusion

This paper presented the results of a parametric analysis on the long-term response of the backfill-abutment system of a semi-integral bridge. A two-dimensional FE model was used to analyze the influence of the completion season of the bridge construction, the stiffness of the bridge foundation, and the lateral displacement amplitude of the bridge abutment on the development of lateral earth pressures on the abutment wall and settlements on the backfill surface. The parametric analysis included annual temperature variations over a 50-year period. The following conclusions can be drawn from the parametric analysis performed as part of this investigation:

1. While the completion season of bridge construction was found not to play a distinguished influence on the lateral earth pressure, the embankment settlement was highly affected by the construction season. Completing the semi-integral bridge construction in summer produced the largest settlements, as compared to the other seasons. Conversely, winter was found to be the best period to complete construction. The maximum settlement in summer was about 47% larger than that in winter.
2. Variations in piling foundation stiffness caused a very low impact on the cyclic response of the backfill-abutment system of the assessed semi-integral bridge. An increase of 224% in the flexural stiffness of the pile foundation resulted in a reduction of only 8% in the peak wall reaction ratio on the abutment wall and 5% in the normalized maximum settlement of the backfill surface at Cycle no. 50.
3. The backfill-abutment system was significantly influenced by the magnitude of the lateral displacement amplitude of the abutment. Lower amplitudes caused lateral earth pressures to decrease with the cycles, while higher amplitudes led to an escalation of lateral earth pressures in initial cycles and stabilization in subsequent cycles. The results suggest that there is a specific amplitude for which earth pressures are not influenced by the cyclic abutment movements. On the other hand, settlements followed an increasing path with the cycles, for any amplitude.
4. The magnitude of the displacement amplitude influenced the development of deformation patterns within the backfill soil mass. Soil shearing prevailed over soil densification under lower amplitudes, while a balance between both shearing and densification was reached under higher amplitudes. More shearing under lower amplitudes resulted in lower lateral earth pressures on the abutment and higher settlements on the backfill surface with the cycles. On the other hand, the balanced effect between shearing and densification attained under larger amplitudes resulted in stabilization of lateral earth pressures and increase of settlements with the cycles.
5. The outcome of the present investigation suggests that abutment backfills of shorter bridges would be more prone to settlement variations caused by changes in the lateral displacement magnitude. This would not be the case for longer bridges, for which backfill settlements would be much less dependent on lateral displacement magnitude variations.

The findings from this investigation could prove useful in assisting decision-making processes in the design and construction of semi-integral bridge abutments. The results indicate that the season of the year the bridge is completed can play an important role on the future performance of the bridge abutment undergoing cyclic loading. Therefore, planning to complete bridge construction in the most appropriate time of year could help reduce potential damage in the abutment backfills and approach slabs. These results can provide insights into the choice for suitable design earth pressures on the abutments, according to the bridge length and the predicted lateral movement variations. A glimpse into how the magnitudes of the predicted lateral movements could impact the development of backfill settlements can also be discerned from the outcome of the present study. Finally, this work also draws attention to the possibility of using more flexible foundations with semi-integral bridges in situations where rigid foundations are not strictly required, since it was observed that the foundation stiffness had only a small impact on the behavior of the soil-abutment system. The suggested analysis methodology could be applied when revising SIAB design guidelines. However, it is important to point out that the present study has analyzed the case of a particular semi-integral abutment, and further analyses are required to better understand the behavior of semi-integral bridges under different structural, geological, geotechnical, and environmental conditions.

Data Availability Statement

Some or all data, models, or codes that support the findings of this study are available from the corresponding author upon reasonable request.

Acknowledgments

This research was sponsored by the National Council for Scientific and Technological Development (CNPq), Brazil (Grant Nos. 429217/2018-8 and 310254/2021-3) and the Texas Department of Transportation (TxDOT) (Project 0-6936). Financial support is gratefully acknowledged.

References

AASHTO. 2017. *LRFD bridge design specifications*. Washington, DC: AASHTO.

Abdel-Fattah, M. T., and T. T. Abdel-Fattah. 2019. "Behavior of integral frame abutment bridges due to cyclic thermal loading: Nonlinear finite-element analysis." *J. Bridge Eng.* 24 (5): 04019031. https://doi.org/10.1061/(ASCE)BE.1943-5592.0001394.

Ahmed, S., I. Khoury, S. Sargand, J. Nusairat, W. Hamid, and H. H. Hussein. 2023. "Thermal behavior of a semi-integral abutment bridge with turn-back wingwalls supported on drilled shafts." *J. Perform. Constr. Facil.* 37 (2): 04023001. https://doi.org/10.1061/JPCFEV.CFENG-4255.

Alhowaidi, Y., J. Eun, S. Kim, C. R. Song, and F. Jaber. 2023. "Field monitoring and analysis of abutment foundation behavior for a curved integral abutment bridge under thermal loading." *Transp. Res. Rec.* 2677 (9): 582–593. https://doi.org/10.1177/03611981231159873.

Al-qarawi, A., C. Leo, and D. S. Liyanapathirana. 2020. "Effects of wall movements on performance of integral abutment bridges." *Int. J. Geomech.* 20 (2): 04019157. https://doi.org/10.1061/(ASCE)GM.1943-5622.0001559.

Arsoy, S., R. M. Barker, and J. M. Duncan. 2002. *Experimental and analytical investigations of piles and abutments of integral bridges*. Charlottesville, VA: Virginia Transportation Research Council.

Arsoy, S., J. M. Duncan, and R. M. Barker. 2004. "Behavior of a semiintegral bridge abutment under static and temperature-induced cyclic loading." *J. Bridge Eng.* 9 (2): 193–199. https://doi.org/10.1061/(ASCE)1084-0702(2004)9:2(193).

Banks, J. R., and A. G. Bloodworth. 2018. "Lateral stress profiles on integral bridge abutments." *Proc. Inst. Civ. Eng. Bridge Eng.* 171 (3): 155–168. https://doi.org/10.1680/jbren.17.00017.

Bloodworth, A. G., M. Xu, J. R. Banks, and C. R. I. Clayton. 2012. "Predicting the earth pressure on integral bridge abutments." *J. Bridge Eng.* 17 (2): 371–381. https://doi.org/10.1061/(ASCE)BE.1943-5592.0000263.

Breña, S. F., C. H. Bonczar, S. A. Civjan, J. T. Dejong, and D. S. Crovo. 2007. "Evaluation of seasonal and yearly behavior of an integral abutment bridge." *J. Bridge Eng.* 12 (3): 296–305. https://doi.org/10.1061/(ASCE)1084-0702(2007)12:3(296).

Brinkgreve, R. B. J., S. Kumarswamy, and W. M. Swolfs. 2016. *Plaxis 2D: Reference manual*. Delft, Netherlands: Plaxis bv.

BSI (British Standards Institution). 2011. *PD6694-1:2011—Recommendation for the design of structures subject to traffic loadings to BS EN 1997-1:2004*. London: BSI.

BSI (British Standards Institution). 2014. *BS EN 1997-1:2004+A1:2013—NA to Eurocode 7: Geotechnical design—Part 1: General rules*. London: BSI.

Burke, M. P., Jr. 2009. *Integral & semi-integral bridges*. Oxford, UK: Wiley.

Caristo, A., J. Barnes, and S. A. Mitoulis. 2018. "Numerical modelling of integral abutment bridges under seasonal thermal cycles." *Proc. Inst. Civ. Eng. Bridge Eng.* 171 (3): 179–190. https://doi.org/10.1680/jbren.17.00025.

Civjan, S. A., E. Kalayci, B. H. Quinn, S. F. Breña, and C. A. Allen. 2013. "Observed integral abutment bridge substructure response." *Eng. Struct.* 56: 1177–1191. https://doi.org/10.1016/j.engstruct.2013.06.029.

Clayton, C. R. I., M. Xu, and A. Bloodworth. 2006. "A laboratory study of the development of earth pressure behind integral bridge abutments." *Géotechnique* 56 (8): 561–571. https://doi.org/10.1680/geot.2006.56.8.561.

Cosgrove, E. F., and B. M. Lehane. 2003. "Cyclic loading of loose backfill placed adjacent to integral bridge abutments." *Int. J. Phys. Modelling Geotech.* 3 (3): 9–16. https://doi.org/10.1680/ijpmg.2003.030302.

England, G. L., N. C. M. Tsang, and D. I. Bush. 2000. *Integral bridges: A fundamental approach to the time-temperature loading problem*. London: Thomas Telford.

Farhangi, V., M. Zadehmohamad, A. Monshizadegan, M. A. Izadifar, M. J. Moradi, and H. Dabiri. 2023. "Effects of geogrid reinforcement on the backfill of integral bridge abutments." *Buildings* 13 (4): 853. https://doi.org/10.3390/buildings13040853.

Frosch, R. J., and M. D. Lovell. 2011. *Long-term behavior of integral abutment bridges*. West Lafayette, IL: Purdue Univ.

Gabrieli, F., G. Zorzi, and R. Wan. 2015. "Granular ratcheting phenomena behind a model retaining wall." In *Geomechanics from micro to macro*, edited by K. Soga, K. Kumar, G. Biscontin, and M. Kuo, 601–606. London: Taylor & Francis Group.

Gerdau. 2019. *Steel sheet piling: Quick reference guide*. Midlothian, TX: Gerdau.

Hoppe, E. J., and T. M. Bagnall. 2008. *Performance of a skewed semi-integral bridge: Volume 1: Field monitoring*. Charlottesville, VA: Virginia Transportation Research Council.

Huang, F., Z. Liu, D. Song, Z. Lin, and B. Chen. 2022. "Test on interaction of semi-integral abutment and soil based on displacement effect of medium-long-term ambient temperature." *J. Traffic Transp. Eng.* 22 (5): 131–144. https://doi.org/10.19818/j.cnki.1671-1637.2022.05.007.

Huntley, S. A., and A. J. Valsangkar. 2013. "Field monitoring of earth pressures on integral bridge abutments." *Can. Geotech. J.* 50 (8): 841–857. https://doi.org/10.1139/cgj-2012-0440.

Husain, I., and D. Bagnariol. 1996. *Integral abutment bridges*. Toronto: Ronen House.

Husain, I., and D. Bagnariol. 1999. *Semi-integral abutment bridges*. Toronto: Queen's Printer for Ontario.

Hussein, H. H., I. Khoury, and J. S. Lucas. 2022. "Environment-induced performance of end concrete diaphragm in skewed semi-integral bridges." *Buildings* 12 (11): 1985. https://doi.org/10.3390/buildings12111985.

Jaky, J. 1944. "The coefficient of earth pressure at rest." [In Hungarian.] *J. Soc. Hung. Eng. Arch.* 78: 355–358.

Kim, S., J. Ahn, C. Jung, J. Jang, and Y. Park. 2014. "Behaviour of steel-box semi-integral abutment bridge considering temperature-earth pressure change." *Int. J. Steel Struct.* 14 (1): 117–140. https://doi.org/10.1007/s13296-014-1011-7.

Kim, W., and J. A. Laman. 2012. "Seven-year field monitoring of four integral abutment bridges." *J. Perform. Constr. Facil.* 26 (1): 54–64. https://doi.org/10.1061/(ASCE)CF.1943-5509.0000250.

Liu, H., J. Han, and R. L. Parsons. 2022. "Settlement and horizontal earth pressure behind model integral bridge abutment induced by simulated seasonal temperature change." *J. Geotech. Geoenviron. Eng.* 148 (6): 04022043. https://doi.org/10.1061/(ASCE)GT.1943-5606.0002812.

MassDOT (Massachusetts Department of Transportation). 2020. *LRFD bridge design guidelines*. Boston, MA: MassDOT.

Mitoulis, S. A., A. Palaiochorinou, I. Georgiadis, and S. Argyroudis. 2016. "Extending the application of integral frame abutment bridges in earthquake-prone areas by using novel isolators of recycled materials." *Earthq. Eng. Struct. Dyn.* 45: 2283–2301. https://doi.org/10.1002/eqe.2760.

Mofarraj, B., and J. G. Zornberg. 2022. "Field monitoring of soil-structure interaction in semi-integral bridges." In *Geo-Congress 2022: Advances in monitoring and sensing; embankments, slopes, and dams; pavements; and Geo-education*, edited by A. Lemnitzer and A. W. Stuedlein, 33–42. Charlotte, NC: ASCE.

Ng, C. W. W., S. M. Springman, and A. R. M. Norrish. 1998. "Centrifuge modeling of spread-base integral bridge abutments." *J. Geotech. Geoenviron. Eng.* 124 (5): 376–388. https://doi.org/10.1061/(ASCE)1090-0241(1998)124:5(376).

Rankine, W. J. M. 1857. "On the stability of loose earth." *Philos. Trans. R. Soc. London* 147: 9–27. https://doi.org/10.1098/rstl.1857.0003.

Salkind, N. J. 2017. *Statistics for people who (think they) hate statistics*. Thousand Oaks, CA: SAGE.

Schanz, T., P. A. Vermeer, and P. G. Bonnier. 1999. "The hardening soil model: Formulation and verification." In *Beyond 2000 in computational geotechnics: Ten years of Plaxis international*, edited by R. B. J. Brinkgreve, 281–296. Rotterdam, Netherlands: A.A. Balkema.

Shid Moosavi, S. S., and A. R. Rahai. 2018. "The performance of integral and semi-integral pre-tensioned concrete bridges under seismic loads in comparison with conventional bridges." *Aut J. Civil Eng.* 2 (2): 219–226. https://doi.org/10.22060/AJCE.2018.14338.5473.

Silva, P. H. S., Y. D. J. Costa, J. R. Walter, B. M. Kouchaki, J. G. Zornberg, and C. M. L. Costa. 2023. "Numerical evaluation of a semi-integral bridge abutment under cyclic thermal movements." *Transp. Geotech.* 39: 100938. https://doi.org/10.1016/j.trgeo.2023.100938.

Springman, S. M., A. R. M. Norrish, and C. W. W. Ng. 1996. *Cyclic loading of sand behind integral bridge abutments*. Workingham, UK: Transport Research Laboratory.

Steinberg, E., S. M. Sargand, and C. Bettinger. 2004. "Forces in wingwalls of skewed semi-integral bridges." *J. Bridge Eng.* 9 (6): 563–571. https://doi.org/10.1061/(ASCE)1084-0702(2004)9:6(563).

Tatsuoka, F., D. Hirakawa, M. Nojiri, H. Aizawa, H. Nishikiori, R. Soma, M. Tateyama, and K. Watanabe. 2009. "A new type of integral bridge comprising geosynthetic-reinforced soil walls." *Geosynth. Int.* 16 (4): 301–329. https://doi.org/10.1680/gein.2009.16.4.301.

TxDOT (Texas Department of Transportation). 2020. *Geotechnical manual*. Austin, TX: TxDOT.

Vipulanandan, C., A. J. Puppala, M. Jao, M. S. Kim, H. Vasudevan, P. Kumar, and Y. L. Mo. 2008. *Correlation of Texas cone penetrometer test values and shear strength of Texas soils: Technical report*. Houston: Univ. of Houston.

Zadehmohamad, M., J. B. Bazaz, R. Riahipour, and V. Farhangi. 2021. "Physical modeling of the long-term behavior of integral abutment bridge backfill reinforced with tire-rubber." *Int. J. Geotech. Eng.* 12: 36. https://doi.org/10.1186/s40703-021-00163-2.

Zornberg, J. G., B. Mofarraj, Y. Costa, P. Silva, and T. Helwig. 2019. *TxDOT project 0-6936: Development of integral/semi-integral abutments for Texas bridges*. Austin, TX: Univ. of Texas at Austin.